Published in final edited form as:
*Dev Cell*. 2014 February 10; 28(3): 282–294. doi:10.1016/j.devcel.2013.12.014.

# BuGZ is required for Bub3 stability, Bub1 kinetochore function, and chromosome alignment

**Chad M. Toledo**[1,3,*], **Jacob A. Herman**[4,*], **Jonathan B. Olsen**[5], **Yu Ding**[1], **Philip Corrin**[1], **Emily J. Girard**[2], **James M. Olson**[2], **Andrew Emili**[5], **Jennifer G. DeLuca**[4,†], and **Patrick J. Paddison**[1,3,†]

[1]Human Biology Division, Fred Hutchinson Cancer Research Center, Seattle, WA 98109, USA

[2]Clinical Research Division, Fred Hutchinson Cancer Research Center, Seattle, WA 98109, USA

[3]Molecular and Cellular Biology Program, University of Washington, Seattle, WA 98195, USA

[4]Department of Biochemistry and Molecular Biology, Colorado State University, Fort Collins, CO 80523, USA

[5]Donnelly Centre for Cellular and Biomolecular Research, University of Toronto, ON, M5S 3E1, Canada

## Summary

During mitosis, the spindle assembly checkpoint (SAC) monitors the attachment of kinetochores (KTs) to the plus ends of spindle microtubules (MTs) and prevents anaphase onset until chromosomes are aligned and KTs are under proper tension. Here, we identify a SAC component, BuGZ/ZNF207, from an RNAi viability screen in human Glioblastoma multiforme (GBM) brain tumor stem cells. BuGZ binds to and stabilizes Bub3 during interphase and mitosis through a highly conserved GLE2p-binding sequence (GLEBS) domain. Inhibition of BuGZ results in loss of both Bub3 and its binding partner Bub1 from KTs, reduction of Bub1-dependent phosphorylation of centromeric histone H2A, attenuation of KT-based Aurora kinase B activity, and lethal chromosome congression defects in cancer cells. Phylogenetic analysis indicates that BuGZ orthologs are highly conserved among eukaryotes, but are conspicuously absent from budding and fission yeasts. These findings suggest BuGZ has evolved to facilitate Bub3 activity and chromosome congression in higher eukaryotes.

### Keywords

BuGZ; ZNF207; Bub3; spindle assembly checkpoint; kinetochore; cancer stem cells; Glioblastoma multiforme

†Correspondence: Patrick Paddison (paddison@fhcrc.org) or Jennifer DeLuca (Jennifer.Deluca@ColoState.edu).
*These authors contributed equally to this work.

## Introduction

During mitosis, the spindle assembly checkpoint (SAC) monitors the attachment of kinetochores (KTs) to the plus ends of spindle microtubules (MTs) and prevents anaphase onset until chromosomes are aligned and KTs are under proper tension (Lara-Gonzalez et al., 2012; Santaguida and Musacchio, 2009). The SAC machinery contains multiple KT proteins (i.e., Bub1, BubR1, Bub3, Mad1, Mad2, and Mps1) that monitor MT attachment and regulate anaphase progression (Lara-Gonzalez et al., 2012; Santaguida and Musacchio, 2009). The SAC proteins Mad2, BubR1, and Bub3 comprise the soluble Mitotic Checkpoint Complex (MCC) and prevent the activation of the ubiquitin ligase anaphase promoting complex/cyclosome (APC/C) by targeting APC/C's co-factor Cdc20 (Musacchio and Salmon, 2007). Following proper chromosome alignment and tension at the KT, Cdc20 inhibition is released to activate the APC/C, which begins the cascade of events that lead to anaphase (Musacchio and Salmon, 2007).

In addition, Bub1, BubR1, and Bub3 have been implicated in promoting chromosome alignment through regulation of Aurora B kinase (ABK) activity at KTs during chromosome congression (Lampson and Kapoor, 2005; Logarinho et al., 2008; Meraldi and Sorger, 2005). In prometaphase, Bub1 kinase phosphorylates threonine 120 of centromere-bound Histone 2A (pH2A–T120), which facilitates recruitment of ABK to the KT (Ricke et al., 2012; Taylor et al., 1998; Yamagishi et al., 2010). ABK, in turn, phosphorylates KT-MT attachment proteins, which reduces their binding affinity for MTs and prevents the premature stabilization of KT-MT attachments (Cheeseman et al., 2006; DeLuca et al., 2006; DeLuca et al., 2011; Welburn et al., 2010). In contrast to Bub1, BubR1 activity opposes ABK dependent phosphorylation of KT binding factors by recruiting PP2A phosphatase to the KT (Kruse et al., 2013; Suijkerbuijk et al., 2012). The interplay between these opposing activities regulates the formation of stable-end on KT-MT attachments (Kruse et al., 2013; Lampson and Kapoor, 2005; Suijkerbuijk et al., 2012). Bub3 is required to recruit both Bub1 and BubR1 to KTs (Harris et al., 2005; Wang et al., 2001), and Bub3 inhibition results in chromosome congression defects consistent with loss of Bub1 function at KTs (Logarinho et al., 2008).

Bub1 and BubR1 both interact with Bub3 at the KT through highly conserved GLEBS domains (Bailer et al., 1998; Taylor et al., 1998; Wang et al., 2001). These are short disordered regions of about 40 amino acids that form a series of salt bridges between the WD40 domains of Bub3 and two glutamate residues in the GLEBS domain (Larsen et al., 2007). As a result of Bub3 binding, the GLEBS domain undergoes a conformational shift from a disordered to a well-ordered structure with fixed interaction points on the top face of Bub3's WD40 propeller (Larsen et al., 2007). This interaction is critical for Bub3-dependent recruitment of Bub1 and BubR1 to KTs (Harris et al., 2005; Taylor et al., 1998; Wang et al., 2001). For example, a single amino-acid change in BubR1's GLEBS domain (E406K) is sufficient to prevent Bub3 interaction and BubR1's KT localization (Harris et al., 2005).

We have previously found that human Glioblastoma multiforme (GBM) brain tumors, the most common and lethal form of brain cancer, differentially require BubR1's GLEBS domain to suppress lethal consequences of altered KT function by promoting attachment of

MTs to KTs (Ding et al., 2013). Removal of BubR1 from KTs of GBM stem cells (GSCs) or transformed fibroblasts results in lethality due to a lack of KT-MT attachments, while non-transformed cells are unaffected (Ding et al., 2013; Malureanu et al., 2009). Thus, GBM isolates appear to be more sensitive to perturbation of certain activities of SAC proteins than non-transformed cells. This added sensitivity in GSCs has led us to isolate a facilitator of Bub3 function, ZNF207, an uncharacterized C2–H2 zinc-finger domain gene (Hubert et al., 2013; Pahl et al., 1998). Since we implicate ZNF207 below as a key effector of Bub3 function, we rename the gene *BuGZ* (Bub3 interacting GLEBS and Zinc finger domain containing protein). Here, we report that the human *BuGZ/ZNF207* gene encodes a GLEBS domain-containing and KT binding protein that is required for Bub3 stability, Bub1 KT function, and chromosome alignment.

## Results

*BuGZ* was isolated from an RNAi screen targeting putative human transcription factors to identify key regulators of GSC's expansion and survival. As with our previous studies (Ding et al., 2013; Hubert et al., 2013), we compared GSCs screen results with those from non-transformed human neural stem cells (NSCs), a candidate cell of origin for GBM, to identify GBM-specific lethality hits (Figure 1A). We found *BuGZ* shRNAs in this category. Thus, we set out to validate *BuGZ* as a candidate cancer lethal gene and then attempted to ascertain its cellular function.

Figures 1A–D show that, consistent with the screen data, *BuGZ* knockdown results in differential growth inhibition of GSCs when compared to proliferating human NSCs. Multiple shRNAs provided robust GSC-specific growth inhibition and penetrant knockdown in both GSCs and NSCs (also Figure S1A). Knockdown of KIF11/Eg5 was used as a positive proliferation control. Its inhibition blocks growth of cultured cells regardless of transformation status (Figures 1B and 1F)(Ding et al., 2013; Hubert et al., 2013).

*BuGZ* knockdown also inhibited the growth of SSEA1+ GSC subpopulations, which are enriched for tumor initiating cell activity (Son et al., 2009) (Figure 1E), and inhibited tumor sphere formation, a surrogate assay for stem cell self-renewal (Galli et al., 2004; Singh et al., 2004) (Figure S1B). However, *BuGZ* knockdown did not alter expression of SSEA1 or other progenitor markers, including SOX2 and NESTIN, or neural lineage markers, including GFAP and TUJ1 (data not shown). Moreover, *BuGZ*-knockdown-insensitive-NSCs could be converted to sensitive by genetic transformation with hTERT, dominant-negative $p53^{DD}$, CyclinD1, $CDK4^{R24C}$, H-RasV12, and MYC (Hubert et al., 2013; Kendall et al., 2005) (Figure 1F). Other GSC patient isolates also showed sensitivity to *BuGZ* knockdown, demonstrating that the effect is not patient-specific (Figure 1F). Finally, we performed an *in vivo* competition experiment to directly test the effects of *BuGZ* suppression in an orthotropic xenograft model of GBM by mixing GSCs containing GFP-expressing *shBuGZ* or shControl with non-shRNA control GSCs at an approximate 9:1 ratio respectively (Hubert et al., 2013). Following 17 days post injection, non-shRNA control GSCs drastically outcompeted *shBuGZ* GSCs, while shControl GSCs comprised the bulk tumor mass (Figures 1G and S1C). Thus, *BuGZ* expression is required for GBM tumor formation *in vivo*. Taken

together, these results suggest that GSCs have a differential requirement for *BuGZ*, which is likely driven by oncogenic activity.

To gain insight into the molecular function of BuGZ, we next performed affinity purification mass spectrometry to identify candidate protein binding partners (see Supplemental Experimental Procedures for details). This analysis revealed Bub3 as the top-scoring hit (Figure 2A and Table S1). We confirmed this interaction in reciprocal co-immunoprecipitation experiments. BuGZ was able to pull down Bub3 and vice versa in GSCs (Figure 2B) and 293T cells (Figure S2), demonstrating the proteins interact in cells.

Since SAC signaling is an essential and highly conserved process, we performed phylogenetic analysis to identify *BuGZ* orthologs and examine available data on their function in model genetic systems. *BuGZ* shows strong conservation among eukaryotes with the exception of budding and fission yeasts, where no orthologs could be identified (Figure 2C) (Powell et al., 2012). This is in contrast to Bub3, which is highly conserved in all eukaryotes, including budding and fission yeasts, where it was first identified (Hoyt et al., 1991). Additionally, examination of protein-protein interaction databases available for humans, worms, flies, and plants revealed additional evidence for *BuGZ* ortholog interaction with Bub3 from genome-scale yeast two-hybrid screens or mass spectrometry analysis (Table S2). However, other candidate proteins identified in our mass-spectrometry analysis were not found. This suggests that BuGZ-Bub3 interactions are highly conserved among higher eukaryotes.

We next examined whether BuGZ interacts with Bub3 through a GLEBS domain, similar to Bub1 and BubR1. We observed that *BuGZ* orthologs also harbor a single conserved GLEBS domain motif (AA 344–376 for human), which contains the characteristic two glutamate residues found in all GLEBS domains (AA 358 and 359 for human *BuGZ*) (Figure 2D). Furthermore, mutational analysis of human *BuGZ* followed by immunoprecipitations revealed that BuGZ's GLEBS domain is required for interaction with Bub3, while its zinc finger domains are dispensable (Figures 2E and 2F). Thus, similar to Bub1 and BubR1, BuGZ interacts with Bub3 through a GLEBS domain.

To further explore the role of BuGZ-Bub3 binding, we evaluated the protein levels of each binding partner after RNAi depletion. We found that depletion of BuGZ led to ~2-fold depletion of Bub3 protein in GSCs, NSCs, and HeLa cells, while other SAC and KT proteins (including Bub1, BubR1, Mad2L1, Hec1, and Cdc20) were unaffected (Figures 3A, 3B, and S3A–S3C). However, mRNA levels of *BUB3* remain unchanged with *BuGZ* knockdown (Figure 3C), suggesting the effects are not due to transcriptional regulation or to off-target RNAi. In addition, Bub3 loss due to BuGZ depletion can be rescued by overexpressing a *BuGZ* allele that is resistant to the *shBuGZ* (Figure 3D). Moreover, mutational analysis revealed that the glutamic acid residues E358 and E359 of BuGZ's GLEBS domain are critical for Bub3 stability (Figure 3D). These two glutamic acid residues are invariant among consensus residues for Bub1, BubR1 and Nup98 GLEBS domains (Figure 2D) and are essential for their binding to Bub3 or Rae1 (Bailer et al., 1998; Larsen et al., 2007; Pritchard et al., 1999; Ren et al., 2010; Taylor et al., 1998; Wang et al., 2001).

These results suggest that the BuGZ-Bub3 GLEBS-mediated interaction decreases protein turnover of Bub3.

We next addressed whether BuGZ and Bub3 have overlapping localization patterns in cells. Similar to reports for Bub3 (Taylor et al., 1998), a BuGZ-GFP fusion localized primarily to the nucleus in interphase, concentrated at KTs prior to nuclear envelope breakdown and during early prometaphase, and disappeared from KTs upon MT binding (Figure 3E). Immunostaining of BuGZ revealed a similar localization pattern (Figure S4A). We next determined co-localization patterns of BuGZ and Bub3 in HeLa cells. Bub3, just like BuGZ, maximally localized to KTs prior to nuclear envelope breakdown and remained bound throughout prometaphase as previously described (Howell et al., 2004) (Figure 4A). However, unlike BuGZ, low levels of Bub3 persisted at metaphase KTs.

In contrast to BuGZ and Bub3 KT localization, Bub1 and BubR1, which also associate with Bub3 via GLEBS domains, concentrate at KTs after nuclear envelope breakdown (Figure S4B), consistent with previously published results (Jablonski et al., 1998; Taylor and McKeon, 1997). Similar to these proteins, BuGZ's GLEBS domain is required for KT localization (Figure 4B), while its zinc finger motifs are dispensable (Figure 4B). In addition, depletion of Bub3 using RNAi prevented BuGZ localization to the KT (Figure 4C). Previous reports demonstrated that Bub3, Bub1, and BubR1 all require KNL-1 in order to bind KTs (Kiyomitsu et al., 2007; London et al., 2012; Primorac and Musacchio, 2013; Yamagishi et al., 2012). We found that KNL-1 depletion also resulted in a loss of BuGZ from KTs (Figure 4D). Moreover, when cells were treated with nocodazole, causing spindle MTs to depolymerize, unattached KTs re-accumulated BuGZ (Figure 4E). Conversely, treating cells with taxol, which stabilizes KT-MTs attachments, did not recruit BuGZ to MT-attached KTs (Figure 4E). This behavior is similar to Bub3 and other SAC proteins (Hoffman et al., 2001). Together, these results indicate that BuGZ localizes to KTs by binding to Bub3 through its GLEBS domain and BuGZ's KT localization is regulated by attachment of MTs.

Previous studies report that Bub3 and its binding partners Bub1 and BubR1 exhibit interdependencies for KT localization (Lara-Gonzalez et al., 2012; Santaguida and Musacchio, 2009). We therefore analyzed KT localization of Bub3, Bub1, and BubR1 in BuGZ-depleted HeLa cells. After BuGZ depletion, Bub3 levels are reduced at KTs, which is not unexpected due to the decrease in total protein (Figure 4F). Bub1 KT localization is also significantly decreased (Figure 5A), which is likely due to loss of its obligate KT recruitment factor Bub3 (Taylor et al., 1998; Taylor and McKeon, 1997; Vanoosthuyse et al., 2004). Intriguingly, BubR1 KT association is not affected after BuGZ depletion (Figure 5A), though previous studies have demonstrated that BubR1 KT recruitment relies on Bub3 (Logarinho et al., 2008; Meraldi et al., 2004). It is possible that BubR1 out-competes Bub1 for limiting Bub3 binding sites that remain post-BuGZ depletion, or alternatively, that BuGZ plays a more direct role in Bub1 KT recruitment.

In addition to their well-known roles in SAC signaling, Bub1, BubR1, and Bub3 have also been implicated in facilitating chromosome alignment during mitosis (Lampson and Kapoor, 2005; Logarinho et al., 2008; Meraldi and Sorger, 2005). We therefore examined

chromosome alignment in BuGZ-depleted HeLa cells treated with the proteasome inhibitor MG132 (to prevent precocious anaphase entry), and found that this process was significantly compromised (Figure 5B). In control populations, >95% of cells were able to fully align chromosomes, whereas proper chromosome alignment was observed in less than 55% of BuGZ-depleted cells (Figure 5B). We also detected similar chromosome alignment defects in GSC-0131 and transformed NSC-CB660 upon BuGZ depletion and MG132 treatment (Figure 5C). However, non-transformed NSC-CB660 cells were able to fully align chromosomes following BuGZ loss (Figure 5C). In addition, co-depleting both BuGZ and Bub3 in GSC-0131 resulted in partial to severe chromosome alignment defects similar to BuGZ and Bub3 depletion alone (Figure 5D). The chromosome alignment defects in GSC-131 following depletion of endogenous BuGZ could be rescued by ectopic expression of the *BuGZ* ORF (Figure 5E), which further demonstrates that the chromosome alignment defects are due to BuGZ depletion and not due to off-target RNAi. However, BuGZ GLEBS domain mutations (E358K and E359K) failed to rescue the chromosome alignment defects (Figure 5E). The alignment defects were also observed in live BuGZ-depleted cells, which exhibited significantly extended mitotic transit times (120 min compared to 60 min in control cells) (Figures 5F and S5). Together, these results suggest oncogenic stress alters KT function, which leads to a differential requirement for BuGZ's GLEBS domain in cancer cells for chromosome congression.

To understand the source of these attachment errors, we assayed Bub1 kinase activity, which is implicated in mediating proper chromosome alignment through localization and activation of ABK (Kawashima et al., 2007; Tsukahara et al., 2010; Yamagishi et al., 2010). Bub1 kinase activity was measured in cells by immunostaining its substrate, histone H2AT120. Consistent with loss of Bub1 at KTs, pH2A levels were significantly lower after BuGZ depletion (Figure 6A). Consistent with loss of ABK activity at KTs after BuGZ depletion, we also observed significant loss of phosphorylation of Hec1S44, a critical downstream KT substrate of ABK involved in the regulation of KT-MT attachments (Figure 6A) (DeLuca et al., 2011). Thus, BuGZ affects chromosome alignment by ensuring Bub3 mediated recruitment of Bub1, which in turn ensures appropriate ABK-mediated phospho-regulation of KT-MT attachments.

However, unlike Bub1 and BubR1, BuGZ depleted cells retained a functional SAC response and elicited a significant mitotic delay in response to MT poisons, albeit at diminished levels (Figures 6B and S6). BuGZ and Bub3 co-depleted cells did not sustain a checkpoint arrest under these same conditions, which was similar to the behavior of cells depleted of Bub3 alone (Figure 6C). These results suggest that BuGZ depleted cells have enough residual Bub1 and Bub3 to activate the SAC.

## Discussion

Here, we report that the human *BuGZ/ZNF207* gene encodes a GLEBS domain-containing and KT binding protein that is required for Bub3 stability, Bub1 KT function, and chromosome alignment. A model for BuGZ function is presented in Figure 6D. We propose that BuGZ activity is required for Bub3 stability during interphase and mitosis. BuGZ depletion, therefore, results in a reduction of Bub3 protein levels during interphase and

decreased binding to KTs during mitosis. As a consequence, Bub3-dependent Bub1 recruitment to KTs is compromised. This, in turn, compromises Bub1-dependent recruitment of ABK, which causes lethal chromosome congression defects in cancer cells. Importantly, viability defects and chromosome alignment defects resulting from BuGZ depletion were recreated in non-sensitive cells through oncogenic transformation. This suggests that oncogenic stress can drive an added requirement for BuGZ function in our GBM isolates and other cancer lines.

We previously established that GSCs differentially require BubR1's GLEBS domain to suppress lethal consequences of altered KT function by promoting attachment of MTs to KTs (Ding et al., 2013). Similar to BuGZ, BubR1-GLEBS viability requirement can be reproduced in non-sensitive cells through genetic transformation with RasV12. However, the phenotypes associated with BubR1-GLEBS domain requirement appear to be distinct from those observed for BuGZ. For example, BubR1 knockdown results in severe defects in KT-MT attachment in GBM isolates resulting in short inter-KT distances at metaphase, while BuGZ knockdown results in alignment defects similar to those produced by Bub3 depletion in all GSC isolates (Figure 5E). We postulate that GBM isolates and transformed NSCs have an added requirement for BuGZ due to oncogenic signaling that leads to changes in either KT protein activity (e.g., through changes in stoichiometry) or feedback regulation of genes involved in chromosome congression (e.g., ABK). Based upon these studies, the RTK/Ras pathway is a likely candidate for triggering a BuGZ requirement. The RTK/Ras pathway is over activated in many cancers, including GBM, and there is evidence that Ras-down stream effectors Erk1/2 can directly phosphorylate the C-terminal domain of CENPE, a key KT protein, which is predicted to decrease its MT binding ability (Benanti and Galloway, 2004).

The functional dichotomy between BuGZ and BubR1 is also observed in the SAC. BubR1's essential function is to maintain an intact mitotic checkpoint until all chromosomes are properly aligned and KTs are under proper tension. We observe a significant mitotic delay in cancer cells following depletion of BuGZ despite a significant loss of both Bub1 and Bub3 at the KT (Figures 6B and S6). This mitotic delay is checkpoint dependent as co-depletion of BuGZ and Bub3 prevents mitotic arrest (Figure 6C). Thus, it is likely that unattached KTs present in BuGZ depleted cells are able to generate a functional SAC signal. It is known that Bub1 must be depleted >95% to cause checkpoint abrogation (Meraldi and Sorger, 2005). Therefore, the >40% of Bub3 and Bub1 present in BuGZ depleted cells is likely sufficient for SAC activation.However, we cannot preclude the possibility that BuGZ is also involved in SAC silencing, which contributes to the mitotic delay observed.

Our studies raise a key question: Is BuGZ essential in non-transformed cells? Bub1, Bub3, and BubR1 are all essential for mouse development, as null mutations of these genes cause early embryo lethality (Kalitsis et al., 2000; Malureanu et al., 2009; Perera et al., 2007; Wang et al., 2004). However, the heterozygous state is permissive for normal development, albeit with increases in mitotic abnormalities. Consistent with being non-essential, BubR1's GLEBS domain is not required for mouse embryo fibroblast proliferation or KT-MT attachment (Ding et al., 2013; Malureanu et al., 2009). Our knockdown studies suggest that the hypomorphic BuGZ state is permissive for viability of non-transformed cells, where

Bub3 expression is probably equivalent to Bub3 heterozygous cells. However, we do not know if complete removal of BuGZ would reduce Bub3 levels further, or whether BuGZ will have other essential functions not revealed by our studies (e.g., in its zinc finger domains). It will be also be interesting to see if GLEBS domains are essential for mammalian development, given that our findings suggest targeting GLEBS domain interactions with Bub3 may represent a precision therapy for GBM.

Our findings also raise a critical question regarding BuGZ's role to facilitate Bub3's function: How does BuGZ regulate Bub3's stability? One possibility is that upon Bub3 binding, BuGZ's GLEBS domain masks post-translational modifications of Bub3, such as phosphorylation, ubiquitination, or sumoylation, which prevents it degradation. However, we were unable to detect increases in Bub3 expression from BuGZ depleted cells treated with the proteasome inhibitor MG132 (Figure 3B) or the sumoylation inhibitor ginkgolic acid (data not shown). Another possibility is that BuGZ acts as a molecular chaperone for Bub3 by converting an unfolded or partially folded Bub3 to its final compact and stable confirmation (Larsen et al., 2007), which, for example, may prevent specific proteases from recognizing and degrading unfolded Bub3. Over expression of BuGZ increases the steady-state levels of ectopically expressed and also endogenous Bub3 (Figures 2F and 3D), suggesting that BuGZ expression is rate-limiting for Bub3 stability. Thus, further experimentation is warranted to determine the nature of the change in Bub3 turnover following BuGZ depletion.

Another question is how BuGZ-dependent Bub3 regulation affects Bub1 and BubR1 function at KTs? Bub3 and its binding partners Bub1 and BubR1 exhibit interdependencies for kinetochore localization (Lara-Gonzalez et al., 2012; Santaguida and Musacchio, 2009). Our results suggest that BuGZ loss preferentially depletes Bub1 recruitment to the KT, leaving BubR1 levels unchanged (Figure 5A). This appears to contradict previous studies that have established roles for Bub1 and Bub3 in recruiting BubR1 to kinetochores (Klebig et al., 2009; Liu et al., 2006; Logarinho et al., 2008; Perera et al., 2007; Primorac and Musacchio, 2013; Taylor et al., 1998). However, these studies produce knockdowns of >90% of Bub1 or Bub3. Our studies produce more modest changes in Bub3 levels after BuGZ knock down (Figure 4F) and only partial loss of recruitment of Bub1 to KTs (Figure 5A). This suggests that BubR1 may outcompete Bub1 at KTs for residual Bub3 (e.g., BubR1 could have higher affinity for Bub3 than Bub1). Alternatively, BuGZ could act as an exchange factor facilitating Bub3-Bub1 interactions.

Further, it was recently found that Bub3 KT recruitment is driven by Mps1/TTK-dependent phosphorylation of Knl1's MELT motifs (Kiyomitsu et al., 2007; London et al., 2012; Primorac and Musacchio, 2013; Yamagishi et al., 2012). Consistent with this result, we find that BuGZ KT localization is Knl1-dependent (Figure 4D). Interestingly, Bub3 binding of phosphorylated MELT motifs is ~10-fold greater when Bub1 is present (Primorac et al., 2013). Future work will be required to determine whether BuGZ, Bub1, and BubR1 have similar effects on Knl1-dependent Bub3 KT localization.

In summary, we find that BuGZ is a GLEBS domain-containing and KT binding protein required for Bub3 stability and KT function. In transformed cells, BuGZ knockdown results

in defects in KT-MT attachments and chromosome congression. For cancer biology, these results raise the possibility that inhibiting GLEBS domain interactions with Bub3 may be a therapeutic strategy for refractory cancers like GBM, which suffer from lethal KT-MT instability brought about by oncogenic stress (Ding et al., 2013). For evolutionary biology, these results suggest that BuGZ function may have arisen in higher eukaryotes to facilitate Bub3 function and chromosome congression.

## Experimental Procedures

Western blotting, affinity purification, mass spectrometry, and immunoprecipitations were performed according to standard protocols. Refer to the Supplemental Experimental Procedures for details.

### Cell culture and drug treatment

GSC and NSC lines were grown in N2B27 neural basal media (StemCell Technologies) supplemented with EGF and FGF-2 (20ng/mL each) (Peprotech) on laminin (Sigma) coated polystyrene plates and passaged as described previously (Ding et al., 2013; Hubert et al., 2013). Specifically, cells were detached from their plates using Accutase (Millipore), centrifuged, and resuspended with the appropriate media every 3 to 4 days. 293T and HeLa cells (ATCC) were grown in 10% FBS/DMEM (Invitrogen). Cells were treated with 800nM or 10 μM nocodazole (Sigma) for 24 hours and 1 hour incubations respectively. Taxol (Sigma) was used at 10μM for 24 hours, and MG132 (Tocris) was also used at a final concentration of 10μM. Live cell imaging was performed in Leibovitz's L-15 media (Invitrogen) supplemented with 10% FBS, 7 mM HEPES, pH 7.0 and 4.5 g/l glucose.

### Growth assays

For short-term single clone validation assays, cells were infected with lentivirus containing a single shRNA to the respective gene. Following selection, cells were harvested, counted (NucleoCounter, NBS) and plated in triplicate onto 96-well plates coated with laminin (Ding et al., 2013; Hubert et al., 2013). After 7 days under standard growth conditions with 0.5μg/mL of puromycin to maintain selection and prevent outgrowth of residual uninfected cells, cell proliferative rates were measured using Alamar blue reagent according to manufacture instructions (Invitrogen). For analysis, shRNA containing samples were normalized to their respective shControl samples.

### Western blotting

Western blots were carried out using standard laboratory practices (www.cshprotocols.org), except cells were lysed in a modified RIPA buffer (150mM NaCl, 50mM Tris, pH 7.5, 2mM $MgCl_2$, 0.1% SDS, 2mM DDT, 0.4% deoxycholate, 0.4% Triton X-100, 1X complete protease inhibitor cocktail (complte Mini EDTA-free, Roche), and 1 U/μL benzonase nuclease (Novagen)) at RT for 15 minutes (Chen et al., 2012; Ding et al., 2013; Hubert et al., 2013). Additionally, some cells were subjected to treatment with the protease inhibitor MG-132 (EMD Millipore) at 10μM for 18.5 hours following the infection/selection process. After a shake-off, cells in suspension (mitotic cells) were harvested. Cells remaining attached to the culture plate were washed with PBS to remove the remaining mitotic cells in

culture and detached (interphase/asynchronous cells). Attached cells were then washed with PBS and lysed using the modified RIPA buffer.

### Immunofluorescence

Cells were grown on sterile, acid washed coverslips in 35mm cell culture dishes. Cells were rinsed with PHEM (60mM PIPES, 25nM HEPES, 10mM EGTA, 4mM $MgSO_4$) and either immediately treated with 4% paraformaldehyde for 20 minutes at room temperature, or for phosphorylation specific antibodies, treated with lysis buffer (PHEM+1.0%Triton X-100) for 5 minutes at 37°C and then PFA fixed for 20 minutes at room temperature. Fixed cells were washed, blocked for 1 hour at room temperature in PHEM+10% boiled donkey serum (BDS). Primary antibodies were diluted in PHEM+5% BDS and incubated for 16 hours at 4°C. See Supplemental Experimental procedures for further details.

### Transformed neural stem cells

Normal CB660 neural stems were simultaneously infected with retrovirus containing pbabe-hTERT + p53DD (Addgene, Plasmid 11128), pbabe-cyclinD1 + CDK4R24C (Addgene, Plasmid 11129), and pbabe-c-mycT58A + HRasG12V (Addgene, Plasmid 11130) for three consecutive rounds of infection (Hubert et al., 2013). After recovery, cells were selected with both neomycin for Ras and blasticidin for c-MYC respectively.

### SSEA1+ outgrowth assays

Cells were infected with shControl and *shBuGZ* virus for 48 hours followed by selection with puromycin for 72 hours. Cells were detached from their respective plate, counted with a nucleocounter, and mixed with untreated cells. After mixing, cells were seeded to a 6-well tissue culture dish coated with laminin for further growth. After three days in culture, cells were harvested, counted, seeded to a 6-well tissue culture dish coated with laminin for further growth or washed with cold PBS containing 0.5% bovine serum albumin (BSA) for flow analysis. Cells were analyzed at days 0, 3, 7, 14, and 21. Data analysis was performed using FlowJo (Three Star). See Supplemental Experimental procedures for further details.

### Limiting dilution assay

Cells were infected with shControl or *shBuGZ* virus for 48 hours followed by selection with puromycin for 72 hours (Day 0). Cells were detached from their respective plate, dissociated into single-cell suspensions, counted with a nucleocounter, and then plated into non-tissue culture treated 96-well plates not coated with laminin with various seeding densities (0.125–256 cells per well, 10 wells per seeding density). Cells were incubated at 37˚C for 3 weeks and fed with 10X EGF and FGF-2 neural stem cell expansion media every 3 to 4 days. At the time of quantification, each well was examined for the formation of tumor spheres.

### Xenotransplantation

0827 GSCs were infected with pGIPZ shRNA virus and selected for 3 days in puromycin (1μg/mL). Cells were then harvested using Accutase (Sigma), counted, resuspended in an appropriate volume of culture media, mixed 90% GIPZ plus 10% untreated cells (non-infected cells), and kept on ice prior to immediate transplantation (Hubert et al., 2013).

NOD-scid IL2Rgammanull mice (Jackson Labs #005557) were sedated by inhalation of isoflourane. A small bore hole was made in the skull using a hand drill with a Meisinger #009 steel burr bit (Hager and Meisinger GmbH). $1\times10^5$ cells were slowly injected by pipet into the right frontal cortex approximately 2mm rostral to Bregma, 2mm lateral and 3mm deep through a 0.2–10μL disposable sterile aerosol barrier tip (Fisher Scientific #02–707-30). The burr hole was closed using SURGIFOAM (Johnson & Johnson) and the skin rejoined using TISSUMEND II (Veterinary Product Laboratories, Phoenix, AZ). 17 days after initial transplantation, mice were injected intravenously through the tail with 100μL of 10μM Chlorotoxin: indocyanine green (Blaze Bioscience, Seattle, WA) 4 hours prior to sacrifice by carbon dioxide inhalation. The brain and tumor were removed from the skull and imaged for GFP and indocyanine green fluorescence using the Xenogen IVIS Spectrum imaging system (Caliper Life Sciences).

## Supplementary Material

Refer to Web version on PubMed Central for supplementary material.

## Acknowledgments

We thank Sue Biggins, Jonathan Cooper, Bob Hevner, Robert Bradley, and members of the DeLuca and Paddison labs for helpful discussions; and Pam Lindberg for administrative assistance. This work was supported by the following grants: National Science Foundation Graduate Research Fellowship Program (DGE-0-718124 and DGE-1256082) (CT), Accelerate Brain Cancer Cure (PP), DoD Translational New Investigator Award CA100735 (PP), NIH R21CA170722-01 (PP), NIH P30CA15704 (PP), the Pew Biomedical Scholars Program (JD, PP), a Phi Beta Psi Sorority Cancer Research Grant (PP), and NIH R01 GM088371 (JD).

## References

Bailer SM, Siniossoglou S, Podtelejnikov A, Hellwig A, Mann M, Hurt E. Nup116p and nup100p are interchangeable through a conserved motif which constitutes a docking site for the mRNA transport factor gle2p. EMBO J. 1998; 17:1107–1119. [PubMed: 9463388]

Benanti JA, Galloway DA. The normal response to RAS: senescence or transformation? Cell cycle. 2004; 3:715–717. [PubMed: 15153805]

Cheeseman IM, Chappie JS, Wilson-Kubalek EM, Desai A. The conserved KMN network constitutes the core microtubule-binding site of the kinetochore. Cell. 2006; 127:983–997. [PubMed: 17129783]

Chen X, Skutt-Kakaria K, Davison J, Ou YL, Choi E, Malik P, Loeb K, Wood B, Georges G, Torok-Storb B, et al. G9a/GLP-dependent histone H3K9me2 patterning during human hematopoietic stem cell lineage commitment. Genes Dev. 2012; 26:2499–2511. [PubMed: 23105005]

DeLuca JG, Gall WE, Ciferri C, Cimini D, Musacchio A, Salmon ED. Kinetochore microtubule dynamics and attachment stability are regulated by Hec1. Cell. 2006; 127:969–982. [PubMed: 17129782]

DeLuca KF, Lens SM, DeLuca JG. Temporal changes in Hec1 phosphorylation control kinetochore-microtubule attachment stability during mitosis. J Cell Sci. 2011; 124:622–634. [PubMed: 21266467]

Ding Y, Hubert CG, Herman J, Corrin P, Toledo CM, Skutt-Kakaria K, Vazquez J, Basom R, Zhang B, Risler JK, et al. Cancer-Specific requirement for BUB1B/BUBR1 in human brain tumor isolates and genetically transformed cells. Cancer discovery. 2013; 3:198–211. [PubMed: 23154965]

Galli R, Binda E, Orfanelli U, Cipelletti B, Gritti A, De Vitis S, Fiocco R, Foroni C, Dimeco F, Vescovi A. Isolation and characterization of tumorigenic, stem-like neural precursors from human glioblastoma. Cancer Res. 2004; 64:7011–7021. [PubMed: 15466194]

Harris L, Davenport J, Neale G, Goorha R. The mitotic checkpoint gene BubR1 has two distinct functions in mitosis. Exp Cell Res. 2005; 308:85–100. [PubMed: 15907836]

Hoffman DB, Pearson CG, Yen TJ, Howell BJ, Salmon ED. Microtubule-dependent changes in assembly of microtubule motor proteins and mitotic spindle checkpoint proteins at PtK1 kinetochores. Mol Biol Cell. 2001; 12:1995–2009. [PubMed: 11451998]

Howell BJ, Moree B, Farrar EM, Stewart S, Fang G, Salmon ED. Spindle checkpoint protein dynamics at kinetochores in living cells. Curr Biol. 2004; 14:953–964. [PubMed: 15182668]

Hoyt MA, Totis L, Roberts BT. S. cerevisiae genes required for cell cycle arrest in response to loss of microtubule function. Cell. 1991; 66:507–517. [PubMed: 1651171]

Hubert CG, Bradley RK, Ding Y, Toledo CM, Herman J, Skutt-Kakaria K, Girard EJ, Davison J, Berndt J, Corrin P, et al. Genome-wide RNAi screens in human brain tumor isolates reveal a novel viability requirement for PHF5A. Genes Dev. 2013; 27:1032–1045. [PubMed: 23651857]

Jablonski SA, Chan GK, Cooke CA, Earnshaw WC, Yen TJ. The hBUB1 and hBUBR1 kinases sequentially assemble onto kinetochores during prophase with hBUBR1 concentrating at the kinetochore plates in mitosis. Chromosoma. 1998; 107:386–396. [PubMed: 9914370]

Kalitsis P, Earle E, Fowler KJ, Choo KH. Bub3 gene disruption in mice reveals essential mitotic spindle checkpoint function during early embryogenesis. Genes Dev. 2000; 14:2277–2282. [PubMed: 10995385]

Kawashima SA, Tsukahara T, Langegger M, Hauf S, Kitajima TS, Watanabe Y. Shugoshin enables tension-generating attachment of kinetochores by loading Aurora to centromeres. Genes Dev. 2007; 21:420–435. [PubMed: 17322402]

Kendall SD, Linardic CM, Adam SJ, Counter CM. A network of genetic events sufficient to convert normal human cells to a tumorigenic state. Cancer Res. 2005; 65:9824–9828. [PubMed: 16267004]

Kiyomitsu T, Obuse C, Yanagida M. Human Blinkin/AF15q14 is required for chromosome alignment and the mitotic checkpoint through direct interaction with Bub1 and BubR1. Dev Cell. 2007; 13:663–676. [PubMed: 17981135]

Klebig C, Korinth D, Meraldi P. Bub1 regulates chromosome segregation in a kinetochore-independent manner. J Cell Biol. 2009; 185:841–858. [PubMed: 19487456]

Kruse T, Zhang G, Larsen MS, Lischetti T, Streicher W, Kragh Nielsen T, Bjorn SP, Nilsson J. Direct binding between BubR1 and B56-PP2A phosphatase complexes regulate mitotic progression. J Cell Sci. 2013; 126:1086–1092. [PubMed: 23345399]

Lampson MA, Kapoor TM. The human mitotic checkpoint protein BubR1 regulates chromosome-spindle attachments. Nat Cell Biol. 2005; 7:93–98. [PubMed: 15592459]

Lara-Gonzalez P, Westhorpe FG, Taylor SS. The spindle assembly checkpoint. Curr Biol. 2012; 22:R966–980. [PubMed: 23174302]

Larsen NA, Al-Bassam J, Wei RR, Harrison SC. Structural analysis of Bub3 interactions in the mitotic spindle checkpoint. Proc Natl Acad Sci U S A. 2007; 104:1201–1206. [PubMed: 17227844]

Liu ST, Rattner JB, Jablonski SA, Yen TJ. Mapping the assembly pathways that specify formation of the trilaminar kinetochore plates in human cells. J Cell Biol. 2006; 175:41–53. [PubMed: 17030981]

Logarinho E, Resende T, Torres C, Bousbaa H. The human spindle assembly checkpoint protein Bub3 is required for the establishment of efficient kinetochore-microtubule attachments. Mol Biol Cell. 2008; 19:1798–1813. [PubMed: 18199686]

London N, Ceto S, Ranish JA, Biggins S. Phosphoregulation of Spc105 by Mps1 and PP1 regulates Bub1 localization to kinetochores. Curr Biol. 2012; 22:900–906. [PubMed: 22521787]

Malureanu LA, Jeganathan KB, Hamada M, Wasilewski L, Davenport J, van Deursen JM. BubR1 N terminus acts as a soluble inhibitor of cyclin B degradation by APC/C(Cdc20) in interphase. Dev Cell. 2009; 16:118–131. [PubMed: 19154723]

Meraldi P, Draviam VM, Sorger PK. Timing and checkpoints in the regulation of mitotic progression. Dev Cell. 2004; 7:45–60. [PubMed: 15239953]

Meraldi P, Sorger PK. A dual role for Bub1 in the spindle checkpoint and chromosome congression. EMBO J. 2005; 24:1621–1633. [PubMed: 15933723]

Musacchio A, Salmon ED. The spindle-assembly checkpoint in space and time. Nat Rev Mol Cell Biol. 2007; 8:379–393. [PubMed: 17426725]

Pahl PM, Hodges YK, Meltesen L, Perryman MB, Horwitz KB, Horwitz LD. ZNF207, a ubiquitously expressed zinc finger gene on chromosome 6p21.3. Genomics. 1998; 53:410–412. [PubMed: 9799612]

Perera D, Tilston V, Hopwood JA, Barchi M, Boot-Handford RP, Taylor SS. Bub1 maintains centromeric cohesion by activation of the spindle checkpoint. Dev Cell. 2007; 13:566–579. [PubMed: 17925231]

Powell S, Szklarczyk D, Trachana K, Roth A, Kuhn M, Muller J, Arnold R, Rattei T, Letunic I, Doerks T, et al. eggNOG v3.0: orthologous groups covering 1133 organisms at 41 different taxonomic ranges. Nucleic Acids Res. 2012; 40:D284–289. [PubMed: 22096231]

Primorac I, Musacchio A. Panta rhei: the APC/C at steady state. J Cell Biol. 2013; 201:177–189. [PubMed: 23589490]

Primorac I, Weir JR, Chiroli E, Gross F, Hoffmann I, van Gerwen S, Ciliberto A, Musacchio A. Bub3 reads phosphorylated MELT repeats to promote spindle assembly checkpoint signaling. eLife. 2013; 2:e01030. [PubMed: 24066227]

Pritchard CE, Fornerod M, Kasper LH, van Deursen JM. RAE1 is a shuttling mRNA export factor that binds to a GLEBS-like NUP98 motif at the nuclear pore complex through multiple domains. J Cell Biol. 1999; 145:237–254. [PubMed: 10209021]

Ren Y, Seo HS, Blobel G, Hoelz A. Structural and functional analysis of the interaction between the nucleoporin Nup98 and the mRNA export factor Rae1. Proc Natl Acad Sci U S A. 2010; 107:10406–10411. [PubMed: 20498086]

Ricke RM, Jeganathan KB, Malureanu L, Harrison AM, van Deursen JM. Bub1 kinase activity drives error correction and mitotic checkpoint control but not tumor suppression. J Cell Biol. 2012; 199:931–949. [PubMed: 23209306]

Santaguida S, Musacchio A. The life and miracles of kinetochores. Embo J. 2009; 28:2511–2531. [PubMed: 19629042]

Singh SK, Hawkins C, Clarke ID, Squire JA, Bayani J, Hide T, Henkelman RM, Cusimano MD, Dirks PB. Identification of human brain tumour initiating cells. Nature. 2004; 432:396–401. [PubMed: 15549107]

Son MJ, Woolard K, Nam DH, Lee J, Fine HA. SSEA-1 is an enrichment marker for tumor-initiating cells in human glioblastoma. Cell Stem Cell. 2009; 4:440–452. [PubMed: 19427293]

Suijkerbuijk SJ, Vleugel M, Teixeira A, Kops GJ. Integration of kinase and phosphatase activities by BUBR1 ensures formation of stable kinetochore-microtubule attachments. Dev Cell. 2012; 23:745–755. [PubMed: 23079597]

Taylor SS, Ha E, McKeon F. The human homologue of Bub3 is required for kinetochore localization of Bub1 and a Mad3/Bub1-related protein kinase. J Cell Biol. 1998; 142:1–11. [PubMed: 9660858]

Taylor SS, McKeon F. Kinetochore localization of murine Bub1 is required for normal mitotic timing and checkpoint response to spindle damage. Cell. 1997; 89:727–735. [PubMed: 9182760]

Tsukahara T, Tanno Y, Watanabe Y. Phosphorylation of the CPC by Cdk1 promotes chromosome bi-orientation. Nature. 2010; 467:719–723. [PubMed: 20739936]

Vanoosthuyse V, Valsdottir R, Javerzat JP, Hardwick KG. Kinetochore targeting of fission yeast Mad and Bub proteins is essential for spindle checkpoint function but not for all chromosome segregation roles of Bub1p. Mol Cell Biol. 2004; 24:9786–9801. [PubMed: 15509783]

Wang Q, Liu T, Fang Y, Xie S, Huang X, Mahmood R, Ramaswamy G, Sakamoto KM, Darzynkiewicz Z, Xu M, et al. BUBR1 deficiency results in abnormal megakaryopoiesis. Blood. 2004; 103:1278–1285. [PubMed: 14576056]

Wang X, Babu JR, Harden JM, Jablonski SA, Gazi MH, Lingle WL, de Groen PC, Yen TJ, van Deursen JM. The mitotic checkpoint protein hBUB3 and the mRNA export factor hRAE1 interact with GLE2p–binding sequence (GLEBS)-containing proteins. J Biol Chem. 2001; 276:26559–26567. [PubMed: 11352911]

Welburn JP, Vleugel M, Liu D, Yates JR 3rd, Lampson MA, Fukagawa T, Cheeseman IM. Aurora B phosphorylates spatially distinct targets to differentially regulate the kinetochore-microtubule interface. Mol Cell. 2010; 38:383–392. [PubMed: 20471944]

Yamagishi Y, Honda T, Tanno Y, Watanabe Y. Two histone marks establish the inner centromere and chromosome bi-orientation. Science. 2010; 330:239–243. [PubMed: 20929775]

Yamagishi Y, Yang CH, Tanno Y, Watanabe Y. MPS1/Mph1 phosphorylates the kinetochore protein KNL1/Spc7 to recruit SAC components. Nat Cell Biol. 2012; 14:746–752. [PubMed: 22660415]

## Highlights

- BuGZ is a kinetochore protein that binds to and stabilizes Bub3
- BuGZ localizes to the kinetochore and binds to Bub3 through a conserved GLEBS domain
- BuGZ depletion in transformed cells results in severe chromosome alignment defects
- Inhibiting Bub3's GLEBS domain interactions may be a GBM therapeutic strategy

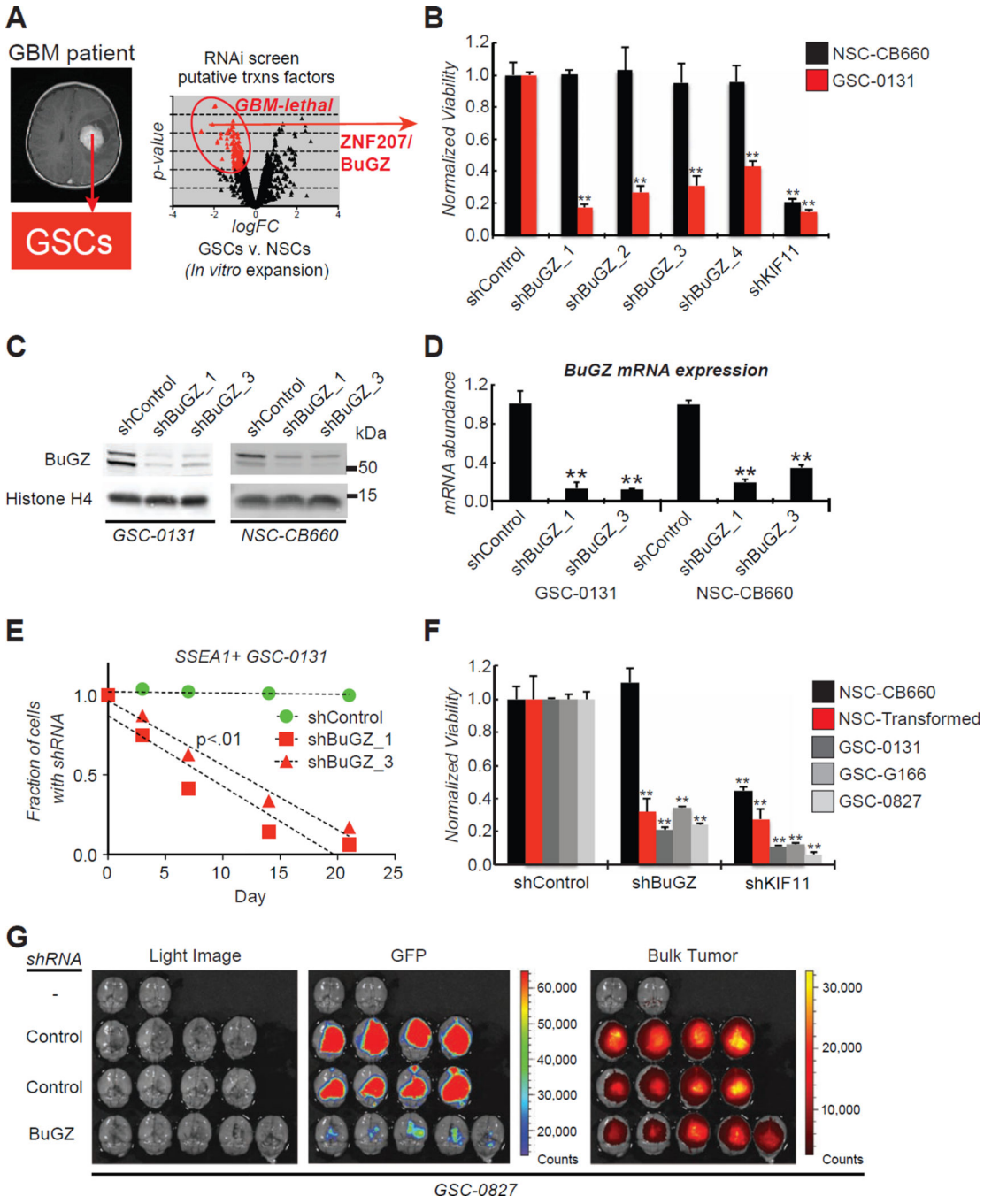


**Figure 1. *BuGZ* is a candidate GBM-lethal gene**

**(A)** An RNAi screen of putative transcription factors revealed *ZNF207/BuGZ* as differentially required for GSC expansion as compared to NSCs.

**(B)***BuGZ* knockdown causes loss of viability in GSCs, but not NSCs. Cells were infected with lentiviruses expressing *BuGZ*, KIF11 or control shRNAs, outgrown for 7 days, and assayed for growth. Knockdown of KIF11 was used as a positive control for both RNAi knockdown and cell proliferation. All viral clones were normalized to their respective shControl. (**Student t test, p<0.01, +SD).

**(C and D)** Western blot analysis and quantitative real time PCR (qRT-PCR) for BuGZ protein and mRNA expression, respectively, of whole cell extracts from GSC-0131 and NSC-CB660 following shRNA knockdown. (**Student t test, $p<0.01$, +SD).

**(E)***BuGZ* knockdown compromises growth of SSEA1+ GSC subpopulations. Flow cytometry analysis of SSEA1+ GSC-0131 cells infected with *shBuGZ*-GFP+ or shControl-GFP+, mixed with untreated cells, and followed for 21 days *in vitro* under self-renewing conditions.

**(F)***BuGZ* knockdown compromises growth of transformed NSCs and multiple GSC isolates, but not NSCs (assay same as (**B**)). (**Student t test, $p<0.01$, +SD).

**(G)** Suppression of *BuGZ* expression compromises GBM tumor formation *in vivo*. Images of *in vivo* competition mouse brains 17 days post orthotopic xenograft of GSC-0827 cells expressing GFP-shControl or GFP-*shBuGZ* mixed with non-shRNA GSC-0827 cells. Right, light images of brains. Middle, GFP+ fluorescence marking shRNA-containing cells. Left, fluorescent signal from Tumor paint (Chlorotoxin: indocyanine green) to identify total tumor mass. First mouse brain of top row did not receive GSC-0827 cells or Tumor Paint, while the second mouse brain of top row did not receive GSC-0827 cells but received Tumor paint. Quantification of GFP fluorescence is shown in Figure S1C. (**Student t test, $p<0.01$). See also Figure S1.

A

**Affinity Purification Mass. Spec.**

| | | GFP | | BuGZ-GFP | |
|---|---|---|---|---|---|
| GENE | kDa | Rep1 | Rep2 | Rep1 | Rep2 |
| BUB3 | 37.2 | 0 | 0 | 92 | 154 |
| GFP | 26.9 | 32 | 53 | 59 | 73 |
| BuGZ | 50.8 | 0 | 0 | 32 | 45 |
| TCOF | 152.1 | 0 | 0 | 31 | 33 |
| SNUT1 | 90.3 | 0 | 0 | 12 | 17 |
| PRDM13 | 74 | 0 | 0 | 10 | 11 |

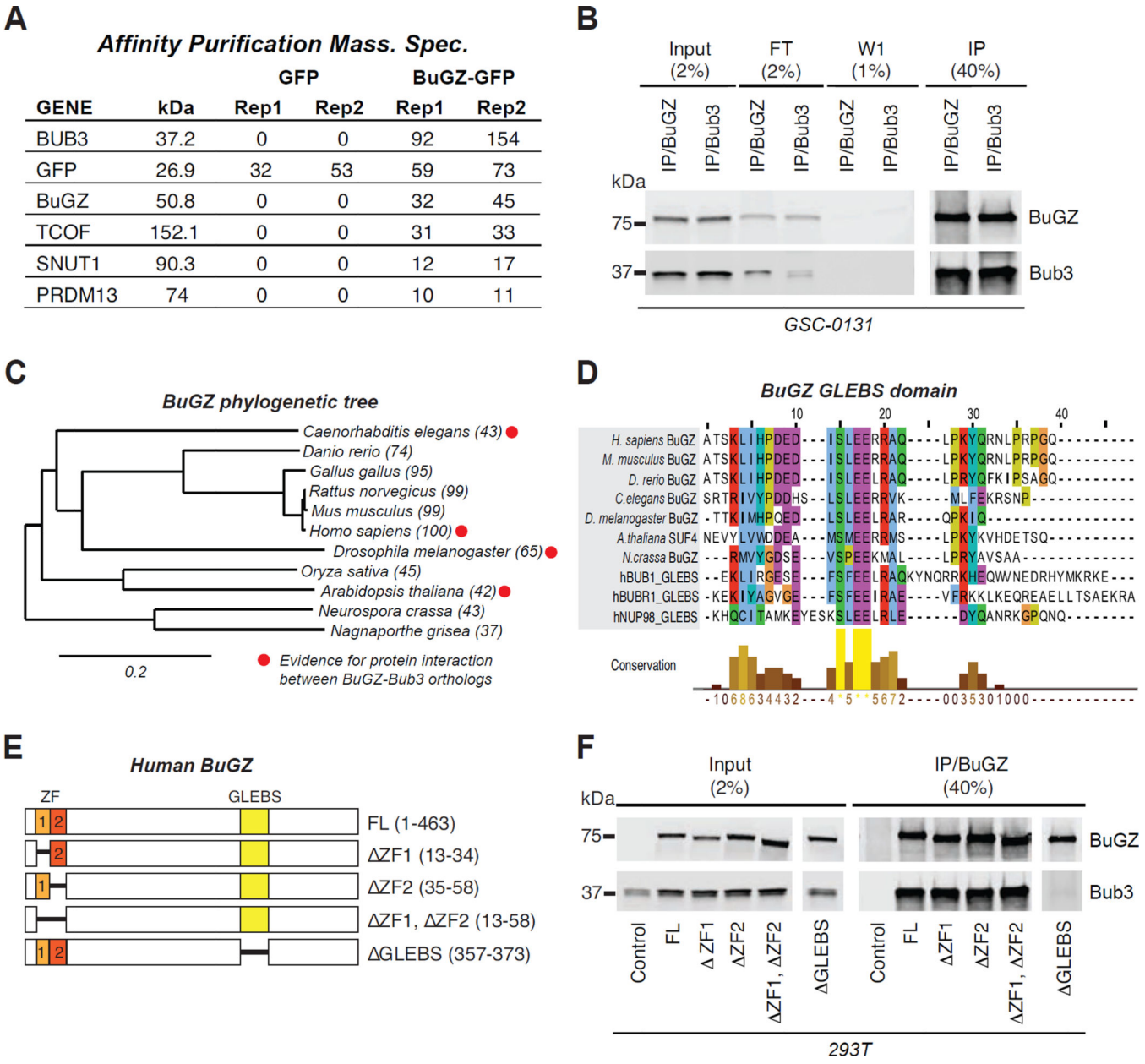


**Figure 2. BuGZ binds to Bub3 through a highly conserved GLEBS domain**

**(A)** Results of affinity purification mass spectrometry of 293T cell extracts transfected with GFP-tagged ZNF207 open reading frame (ORF). Bub3 was identified as the top candidate protein to interact with BuGZ. GFP control ORF was used to identify nonspecific protein interactions. Total results are presented in Table S1.

**(B)** BuGZ binds to Bub3 and vice versa. Western blot analysis with anti-turboGFP (BuGZ) and anti-Bub3 of immunoprecipitates with the turboGFP antibody (BuGZ) or V5 antibody (Bub3) from GSC-0131 cells infected with V5-Bub3 and turboGFP-BuGZ constructs. FT= flow through; W1=wash 1; IP= immunoprecipitation.

**(C)** Evolutionary distance between orthologs of ZNF207/BuGZ sampled from major phyla. Percent protein identify to human BuGZ from pair-wise protein alignments is indicated in parentheses (NCBI, HomoloGene data base). Red dot indicates evidence for BuGZ-Bub3 interactions from protein-protein interaction databases (Table S2).

**(D)** BuGZ orthologs contain a highly conserved GLEBS domain. GLEBS domains from hBub1 (AA240-280), hBubR1 (AA400-440), and hNup98 (157–213) (Larsen et al., 2007; Wang et al., 2001) were used to create pair-wise alignments of indicated BuGZ orthologs using CLUSTW.

**(E)** Human *BuGZ* alleles generated and used in these studies. FL= Full length *BuGZ* open reading frame (ORF); ΔZF1= deletion of first zinc finger motif; ΔZF2= deletion of second zinc finger motif, ΔZF1, ΔZF2= deletion of the two zinc finger motifs; ΔGLEBS= deletion of a portion of the GLEBS motif.

**(F)** BuGZ binds to Bub3 through its GLEBS domain. Western blot analysis with anti-turboGFP and anti-Bub3 of immunoprecipitates with the turboGFP antibody (BuGZ) from 293T cells transfected with the mutant alleles in (**E**) or the control (V5-Bub3). See also Figure S2, Table S1, and Table S2.

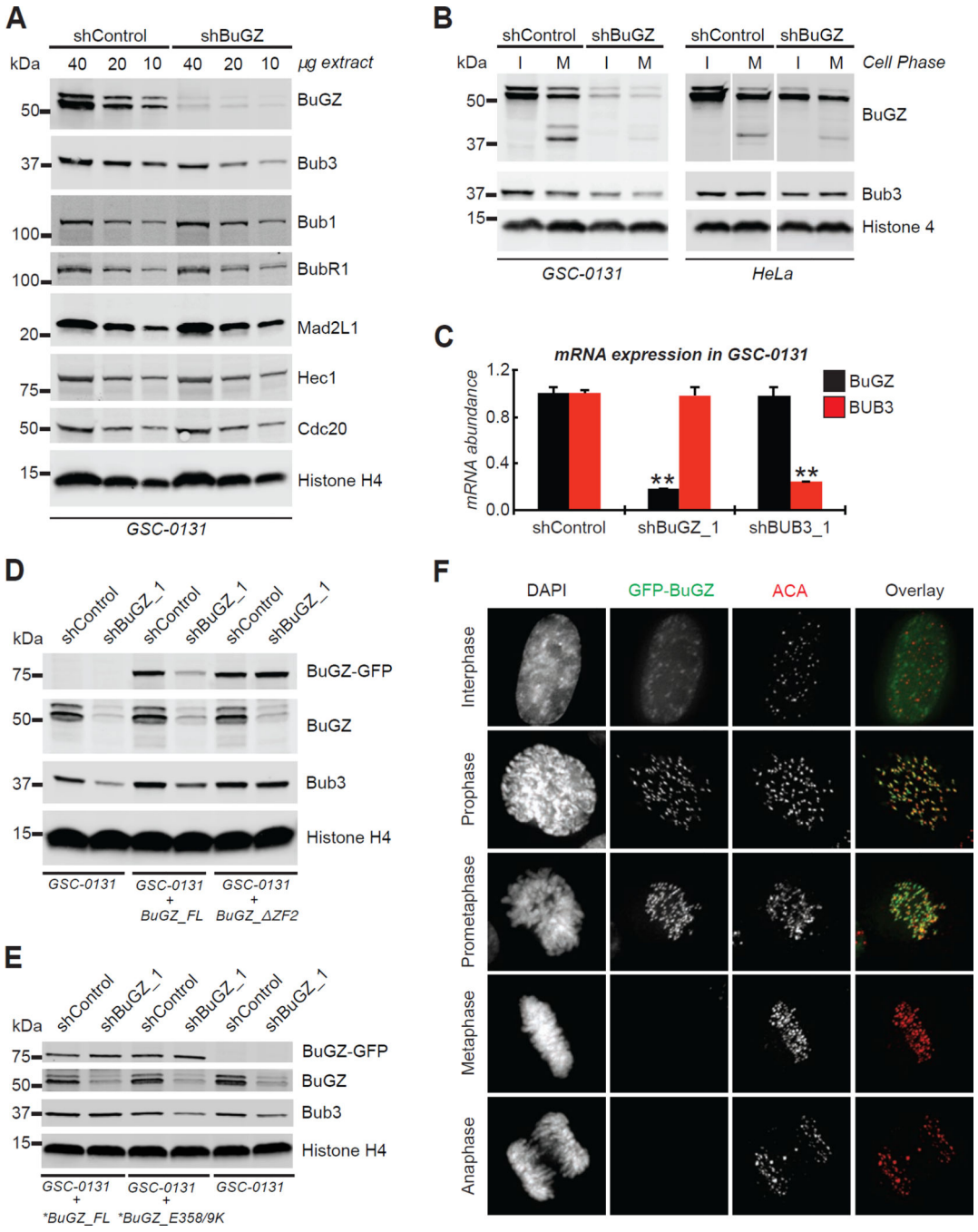


**Figure 3. BuGZ stabilizes Bub3 expression and localizes to the kinetochore**

**(A)** BuGZ stabilizes Bub3 expression. Western blot analysis of GSC-0131 whole cell extracts infected with shControl or *shBuGZ* virus for antibodies to multiple KT-associated proteins and to the loading control anti-Histone H4.

**(B)** BuGZ stabilizes Bub3 expression in interphase and mitotic cells. Western blot analysis of GSC-0131 and HeLa interphase or mitotic cell extracts for anti-BuGZ, anti-Bub3, and loading control anti-Histone H4 antibodies. GSC-0131 cells were infected with shControl or *shBuGZ* virus and treated with the proteasome inhibitor MG-132 for 18.5 hours. HeLa cells were not treated with MG-132. Interphase and mitotic cells were collected by shake-off for both GSC-0131 and HeLa cells. *Mitotic extracts contain additional lower molecular weight species of BuGZ, which could represent a cleavage or degradation product.

**(C)** Knockdown of *BuGZ* does not alter *BUB3* mRNA levels and vice versa. Quantitative real time PCR was used to access *BuGZ* and *BUB3* mRNA expression after shRNA viral infection with shControl, *shBuGZ*, and *shBUB3*. (**Student t test, $p<0.01$, +SD).

**(D)** Expression of BuGZ in BuGZ-depleted GSCs rescues Bub3 expression, but BuGZ-GLEBS domain mutants (E358K E359K) do not. Western blot analysis of GSC-0131 cell extracts for anti-turboGFP, anti-BuGZ, anti-Bub3, and loading control anti-Histone H4 antibodies. GSC-0131 cells were first infected with *BuGZ* ΔZF2 (*shBuGZ*_1 targets the second zinc finger motif), *shBuGZ* resistant (denoted by *) full length (FL) *BuGZ*, or *shBuGZ* resistant *BuGZ* E358K E359K. Following selection, these cells were virally transduced with shControl or *shBuGZ*.

**(E)** BuGZ localizes to KTs in prophase and prometaphase but diminishes during metaphase. HeLa cells were transfected with *GFP-BuGZ* fusions and imaged for DAPI, GFP, and KTs (ACA). Representative images are shown. See also Figure S3.

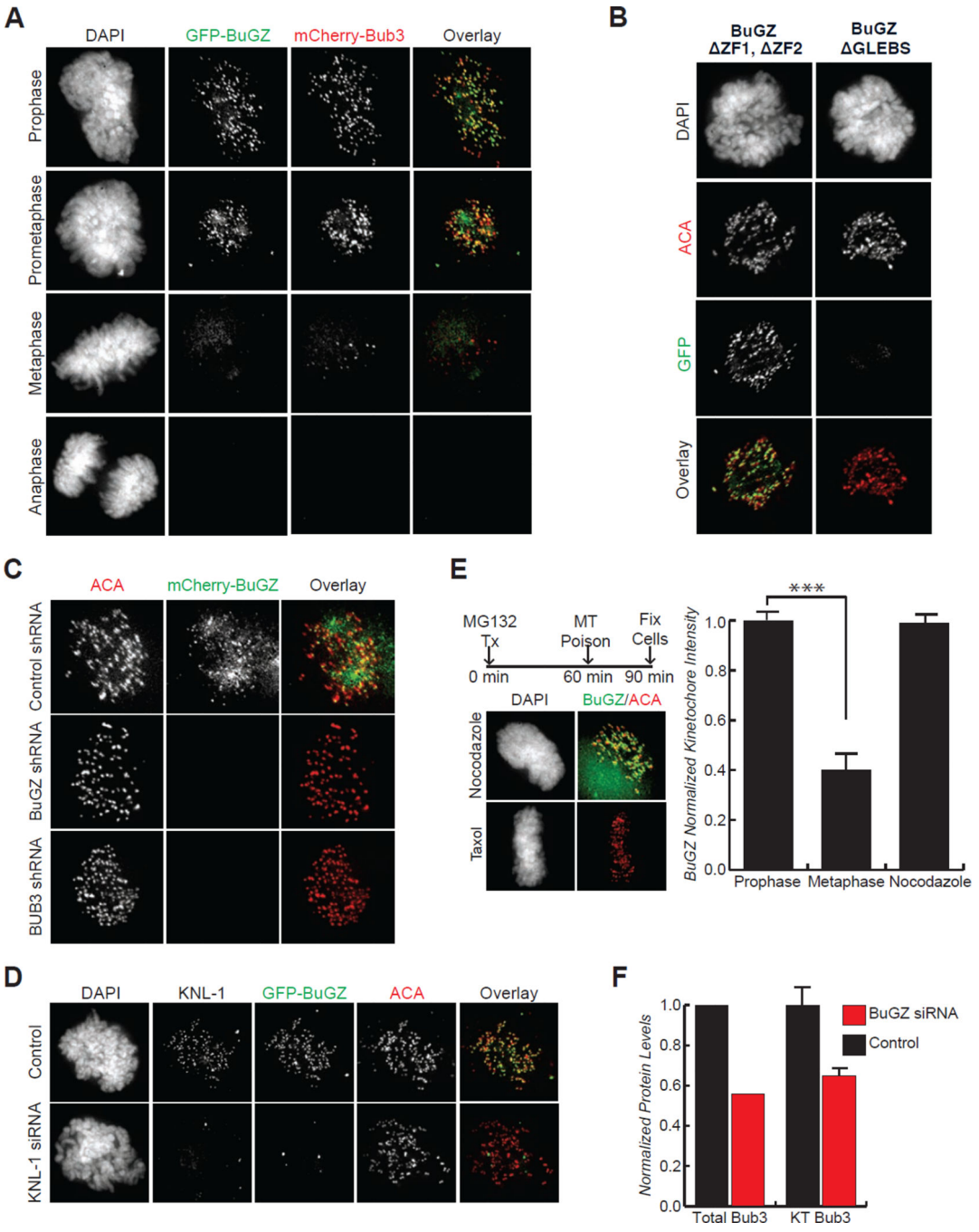


**Figure 4. BuGZ co-localizes with Bub3 at KTs during early mitosis by virtue of its GLEBS domain and reduces Bub3 levels at KTs when inhibited**

**(A)** BuGZ and Bub3 co-localization in HeLa cells transfected with *GFP-BuGZ* and mCherry-BUB3 expression constructs. BuGZ and Bub3 co-localize during prophase and prometaphase. Representative images shown.

**(B)** BuGZ localization in HeLa cells transfected with *GFP-BuGZ* ΔZF1, ΔZF2 or *BuGZ* ΔGLEBS mutants. BuGZ ΔZF1, ΔZF2 localizes to the KTs, while BuGZ ΔGLEBS does not. KTs are stained with anti-centromere antibody (ACA).

**(C)** BuGZ localization is Bub3-dependent. HeLa cells stably expressing BuGZ-mCherry were infected with shControl, *shBuGZ*, or *shBUB3*, selected, and stained with ACA.

**(D)** BuGZ KT localization requires Knl-1. HeLa cells stably expressing BuGZ-GFP were transfected with siControl or siKNL1 and stained with ACA.

**(E)** BuGZ KT binding is regulated by KT-MT attachment. GFP-BuGZ stable Hela cells were treated as shown with Nocodazole or Taxol and imaged.

**(F)** Bub3 total and KT associated protein decreases after BuGZ depletion. Normalized protein levels determined by western blot (left) and immunofluorescence (right). (N=2; error bars represent cellular deviation [control] and experimental deviation [*BuGZ* siRNA]). See also Figure S4.

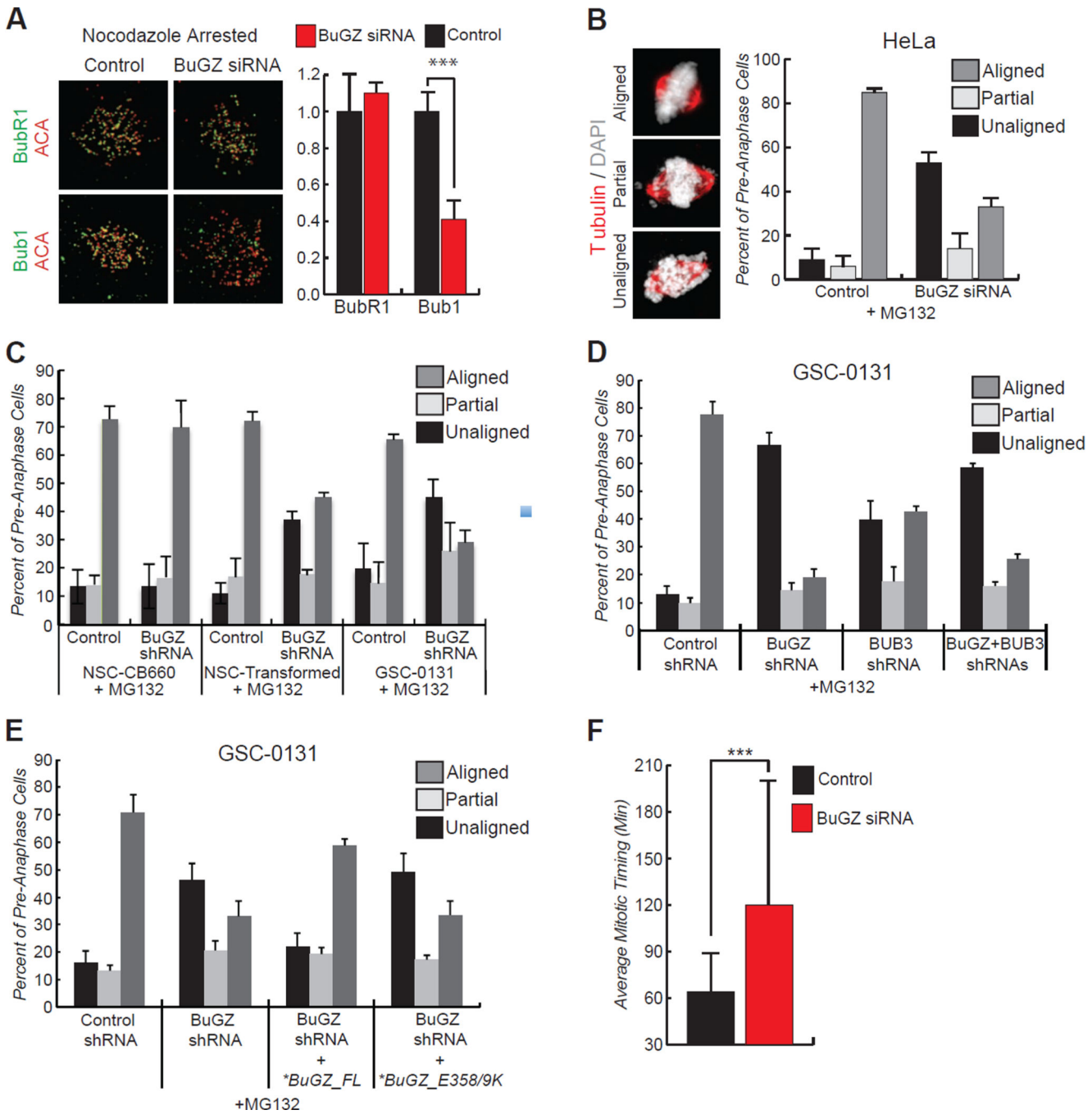


**Figure 5. BuGZ activity is required for proper chromosome alignment**

**(A)** Immunofluorescence analysis of BubR1 and Bub1 KT association. Representative images (left) and quantitative analysis (right) show BuGZ depletion does not alter BubR1 levels, but Bub1 localization significantly reduces (student t test $p<0.001$). Both BubR1 and Bub1 total protein levels are unaltered (Figure 3). (N=2; error bars represent cellular deviation [control] and experimental deviation [*BuGZ* siRNA]).

**(B)** BuGZ depletion causes chromosome alignment defects in HeLa cells. After MG132 treatment, 35% of BuGZ depleted cells align chromosomes compared to 85% of control cells. (>800 cells counted/condition, +SD).

**(C)** BuGZ depletion causes chromosome alignment defects in transformed NSC-CB660 and GSC-0131 cells, but not in non-transformed NSC-CB660 cells. After 2 hours of MG132 treatment, 70% of BuGZ depleted NSC-CB660 cells align chromosomes compared to 45% of BuGZ depleted transformed NSC-CB660 cells. (>395 cells counted/condition, +SD).
**(D)** In GSC-0131 cells, BuGZ and Bub3 co-depletion causes chromosome alignment defects similar to BuGZ and Bub3 depletion alone. After 2 hours of MG132 treatment, 26% of BuGZ/Bub3 co-depleted GSC-0131 cells align chromosomes compared to 19% of BuGZ depleted cells and 43% of Bub3 depleted cells. (>535 cells counted/condition, +SD).
**(E)** Ectopic expression of wild type BuGZ, but not BuGZ GLEBS domain mutants (E358K E359K), rescues chromosome alignment defects in GSCs depleted for endogenous BuGZ. After two hours of MG132 treatment, 59% of BuGZ depleted GSCs expressing *shBuGZ* resistant (denoted by *) full length *BuGZ* display align chromosomes compared to 34% for the *BuGZ* allele containing mutations in the GLEBS domain. (>445 cells counted/condition; +SD).
**(F)** BuGZ depletion delays mitotic timing. HeLa cells expressing H2B–GFP fusion protein were imaged at five minutes intervals to determine time from nuclear envelope breakdown until anaphase onset. BuGZ depleted cells average mitotic timing was 120 minutes compared to 60 minutes in control cells. (***Mann-Whitney test $p<0.001$; $n>60$ cells/condition; +SD). See also Figure S5.

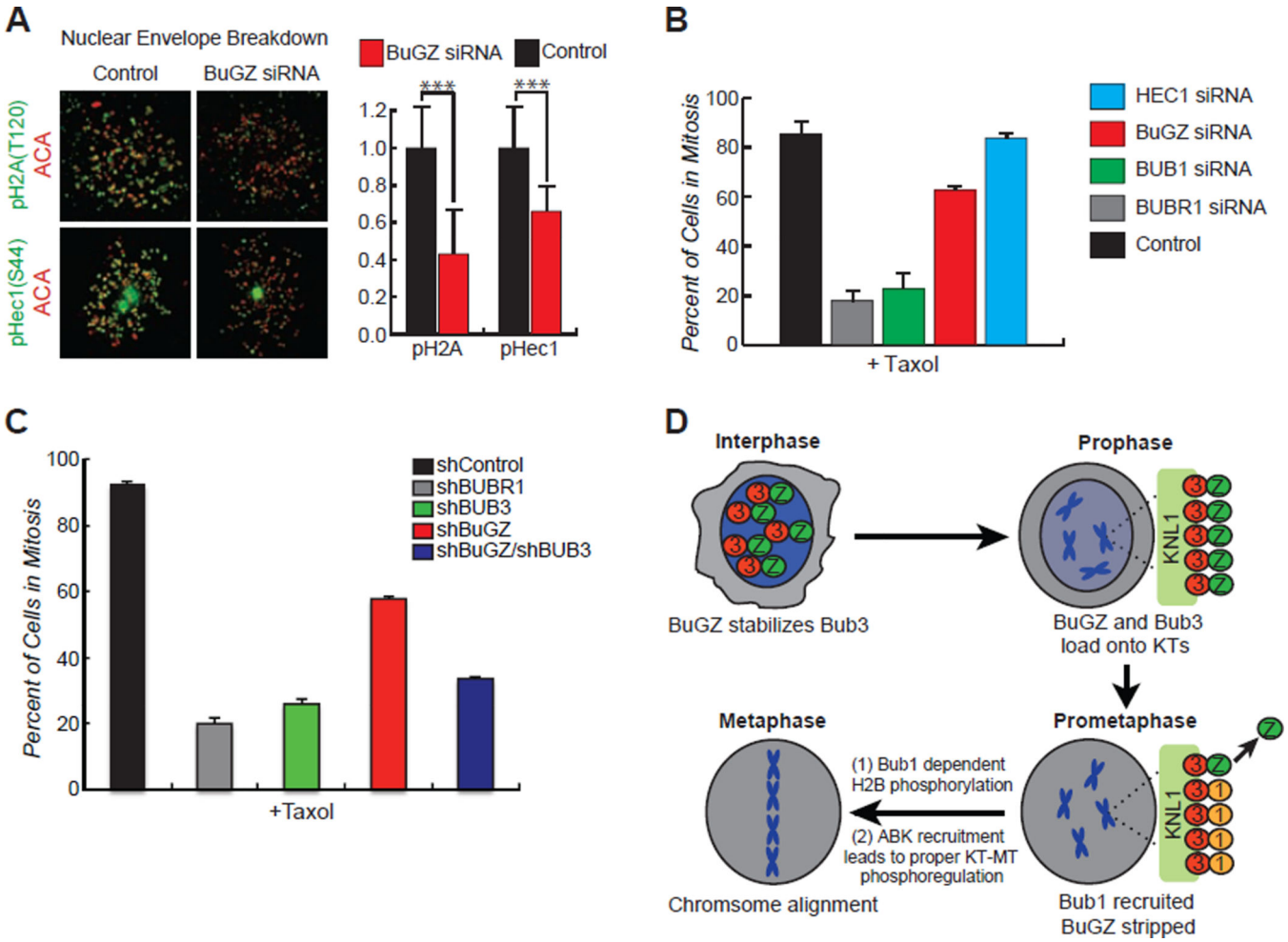


**Figure 6. BuGZ activity is required for localization and activation of ABK, and the spindle assembly checkpoint**

**(A)** Immunofluorescence analysis for kinase activity of Bub1 and Aurora B. Representative images (left) and quantitative analysis (right) show BuGZ depletion decreases phosphorylation of Bub1 and Aurora B substrates, H2A and Hec1 respectively. (***student t test $p<0.001$; N=2; error bars represent cellular deviation [control] and experimental deviation [*BuGZ* siRNA]).

**(B)** BuGZ depleted cells sustain a moderate mitotic arrest in microtubule poisons. A majority of control (black) and attachment factor Hec1 (blue) depleted cells are mitotic after 24 hours in taxol. Depleting SAC proteins BubR1 (gray) and Bub1 (green) causes premature mitotic exit. BuGZ depletion (red) causes an intermediate phenotype, suggesting cells establish a SAC response but cannot maintain it. (N=2; >1000 cells counted/condition; +SD).

**(C)** BuGZ and Bub3 (blue) co-depleted cells do not sustain a checkpoint arrest. A majority of control (black) depleted cells are mitotic after 24 hours in taxol. Depleting SAC proteins BubR1 (gray) and Bub3 (green) causes a premature mitotic exit, while BuGZ depletion (red) causes an intermediate phenotype. Thus, BuGZ induced arrests require checkpoint signaling. (N=3; >1000 cells counted/condition; +SD).

**(D)** Model of BuGZ function. See also Figure S6.